Acc. Chem. Res. **2000,** *33,* 781−789

Measurement of Orientation in Organic Thin Films

GARTH J. SIMPSON† AND KATHY L. ROWLEN*
Department of Chemistry and Biochemistry, University of Colorado, Boulder Colorado 80309

Received April 11, 2000

ABSTRACT
As the potential for applications utilizing oriented thin films grows, so grows the need for accurate, reliable measurements of molecular orientation and surface coverage. Recent work in our laboratory has been directed toward this goal. In this paper the theoretical and experimental effects of surface roughness and the width of the molecular orientation distribution on spectroscopically measured orientation angles are reviewed, the combination of linear and nonlinear spectroscopic techniques for accurate determination of both the mean and width of an orientation distribution is described, and the theory and methodology necessary to obtain orientation-insensitive surface coverage measurements by second harmonic generation for adsorption isotherm and kinetics investigations are reviewed.

Introduction

Orientation measurements of surface systems can provide unique and useful structural information. Furthermore, for generation of oriented films using self-assembly methodologies, the significant orienting interactions occur one molecular layer at a time. Consequently, full characterization of the chemical interactions leading to ordered monolayer (and subsequent multilayer) formation requires analytical techniques which allow for orientation measurements with submonolayer sensitivity. Additionally, since order can be highly dependent on the external environment, the methods should ideally be applicable under ambient conditions. Two techniques satisfying these rather stringent criteria are angle-resolved absorbance with photoacoustic detection (ARAPD) and second harmonic generation (SHG).

Angle-Resolved Absorbance with Photoacoustic Detection. Work in our laboratory has previously demonstrated that photoacoustic detection allows for angle-resolved absorbance measurements with submonolayer detection limits.[1−3] In photoacoustic experiments, the acoustic signal generated when excited-state molecules decay nonradiatively is measured (rather than beam attenuation). Since the amplitude of the acoustic wave is proportional to both the intensity of excitation and sample absorbance under our experimental conditions,[1−3] photoacoustic spectroscopy offers the combined advantages of sensitivity comparable to that of fluorescence and the near universal utility and simplicity of absorbance detection. From the trend in absorbance (and correspondingly photoacoustic amplitude) as the electric field at the interface is varied, the orientation of a given transition moment within the thin film can be evaluated, and from that, molecular orientation can be determined.[1−3]

Second Harmonic Generation. SHG is the frequency doubling of light. As a second-order nonlinear optical process, SHG is dipole forbidden in bulk isotropic media, and therefore it is selective for oriented films at the interface between such media. Molecular orientation can be deduced from the measured relationship between the polarizations of the linear and nonlinear beams. By nature of the interface specificity, SHG may be used under ambient conditions to probe systems that are otherwise difficult to study, including liquid and buried interfaces.[4−6] In the simplest cases, all that is required for SHG measurements is a pulsed laser source, the means to rotate the plane of polarization, a photon detector, and appropriate optical filters. Even using such simple instruments, submonolayer detection limits are routinely achievable for a wide range of interfacial systems.[4−6]

Recent studies in our laboratory have focused generally on interpreting the relationship between macroscopic orientation measurements and the microscopic interactions between molecules and surfaces. Four such lines of inquiry are the subject of this Account. In the first set of investigations, the influence of surface and interface roughness on macroscopic orientation measurements was considered both theoretically and experimentally. In other work, a study of the dependence of macroscopic measurements on the mean orientation angle and width about that mean uncovered the existence of an SHG magic angle. Experimental evaluation of both the means and widths of orientation distributions was demonstrated by combining SHG and ARAPD measurements. Additionally, a new technique has been developed to obtain adsorption isotherm and kinetics measurements by SHG without complications associated with coverage-dependent changes in orientation.

Influence of Surface Roughness on Orientation Measurements

The convenience and optical transparency of fused silica and glass make them attractive and widely used substrates for oriented thin film assembly. While optically flat, such mechanically polished surfaces typically exhibit micro-

Garth J. Simpson obtained his B.S. in Chemistry at Western Washington University. He recently completed his Ph.D. in Chemistry from the University of Colorado, Boulder, under the direction of Kathy Rowlen. Garth is currently a Pfizer Fellow of the Life Sciences Research Foundation working with Professor Richard Zare at Stanford University.

Kathy L. Rowlen is currently an Associate Professor in the department of Chemistry and Biochemistry at the University of Colorado, Boulder. She obtained her bachelor's degree in chemistry at a small college in Michigan (Grand Valley State) in 1984 and her Ph.D. in chemistry at the University of Colorado in 1989. Kathy joined the faculty at UC, Boulder, after a one-year postdoctoral research position with Prof. Joel Harris at the University of Utah. Her research interests include analytical chemistry and surface science. She has received the Beckman Young Investigator Award and an NSF Career Award.

* To whom correspondence should be addressed. Phone: (303) 492-5033. Fax: (303) 492-5894. E-mail: rowlen@spot.colorado.edu.
† Current address: Department of Chemistry, Stanford University, Stanford, CA 94305-5080.

10.1021/ar0000307 CCC: $19.00
Published on Web 08/24/2000

scopic roughnesses comparable to or greater than the molecular dimensions of monolayer films. As a result of this microscopic roughness, the "local" surface plane can be tilted with respect to the macroscopic surface plane. Without a method of quantifying and correcting for this effect, orientation measurements made at non-atomically flat solid surfaces and at liquid interfaces may not be representative of the local interfacial interactions.

The first step in quantification of roughness effects in linear and nonlinear orientation measurements is generation of the probability distribution for the tilt angle of the local surface plane.[7] This distribution can be measured directly from analysis of surface topographs acquired by atomic force microscopy (AFM), provided that the separation between points, L, is comparable to or greater than the tip diameter.[7] However, a monolayer film thickness typically ranges between 10 and 40 Å, which is approximately an order of magnitude smaller than a typical AFM tip diameter. The finite size of the tip often prevents direct measurement of the surface tilt angle distribution at the length scales most relevant to monolayer films. This experimental limitation can be overcome for surfaces that exhibit fractal behavior. Fractal analysis allows for extrapolation of roughness measurements acquired at larger length scales (in which the measurements are reliable) down to molecular scales.[7] Using fractal analysis, the roughness parameter, σ_θ (equal to the root-mean-square difference in heights between two points separated by a distance of L divided by that distance), can be determined:[7,8]

$$\sigma_\theta^2(L) = 2(\sigma_\infty/L)^2[1 - \exp[-(L/\xi)^{2H}]] \qquad (1)$$

where H is an exponential scaling parameter with a value between 0 and 1, ξ is the lateral correlation length, and σ_∞ is the asymptotic root-mean-square height evaluated at image sizes much greater than the correlation length. Together with H, ξ determines the lateral distance required in order to "lose memory" of an initial height. The three parameters, σ_∞, ξ, and H, can be evaluated from analysis of the surface topography.[7−9] The separation distance, L, is in general equal to the film thickness or molecular length (more precisely, L is equal to the length scale of the orienting interactions).[7]

At liquid surfaces, σ_θ can be evaluated from descriptions of interfacial roughness employing capillary wave theory:[10]

$$\sigma_\theta^2(L) = \frac{k_B T}{2\pi L^2 \gamma_\infty} \ln\left[\frac{k_{max}^2(\gamma_\infty + k_L^2(3k_B T/8\pi))}{k_L^2(\gamma_\infty + k_{max}^2(3k_B T/8\pi))}\right] \qquad (2)$$

in which k_{max} is the magnitude of the radial wavevector for a smallest wavelength capillary wave contributing to interfacial roughness (roughly equal to π divided by the size of the solvent molecule), k_B is the Boltzmann constant, T is the temperature, γ_∞ is the macroscopic surface tension, and k_L is equal to π/L. From the value of σ_θ evaluated for a given value of L either from fractal analysis of the surface topography or from capillary wave theory, the probability distribution in local surface normal tilt angles can be generated.[8,10]

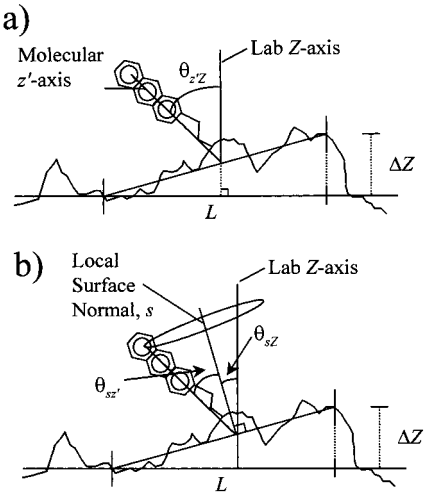

FIGURE 1. Schematic showing relevant angles in the treatment of roughness contributions to linear dichroism. (a) The macroscopic orientation angle, $\theta_{z'Z}$, is the angle between the laboratory Z-axis and the molecular z'-axis, with the z'-axis being the principal orientation axis of the surface-bound molecule. (b) The macroscopic angle $\theta_{z'Z}$ is a function of the two angles, θ_{sZ} (related to surface roughness) and $\theta_{sz'}$ (the local molecular orientation angle). In practice, θ_{sZ} is evaluated from the surface gradient rather than the slope as shown.

Angle-Resolved Absorbance. Once the value of σ_θ has been determined, the influence of roughness on a given measurement may be evaluated. For absorbance measurements, the mathematical expressions necessary for quantification of the influence of roughness are fairly straightforward. For a surface-bound chromophore with a transition moment parallel to the orientation axis (typical for rodlike molecules), the relationship between the macroscopic measurement, surface roughness, and local molecular orientation can be summarized by the compact expression:[11]

$$K_{z'Z} = \frac{1}{2}[1 - K_{sZ} - K_{sZ'} + 3K_{sZ}K_{sZ'}] \qquad (3)$$

in which each value of K_{ij} is equal to $\langle\cos^2\theta_{ij}\rangle$, and the subscripts indicate the relevant angle, such that $\theta_{z'Z}$ is the angle between the molecular orientation axis, z', and the macroscopic surface normal, Z (i.e., the angle probed by spectroscopic orientation measurements), θ_{sZ} is the angle between the local surface normal (indicated by s) and the macroscopic surface normal (i.e., the angle related to surface roughness), and $\theta_{sz'}$ is the molecular orientation angle with respect to its local environment. Note that for cases in which the transition moment is not parallel with the molecular orientation axis, a more general form of eq 3 can be written by substituting $K_{sz'}$ with K_{sf}, which describes the angle between the local surface normal and the transition moment, f. Expressions are given in ref 11 to evaluate molecular orientation using the value for K_{sf}. The relationships between the various angles are depicted schematically in Figure 1.

For moderately rough surfaces and interfaces, such that $\sigma_\theta \leq \sim 1/2$, the value of K_{sZ} can be reasonably ap-

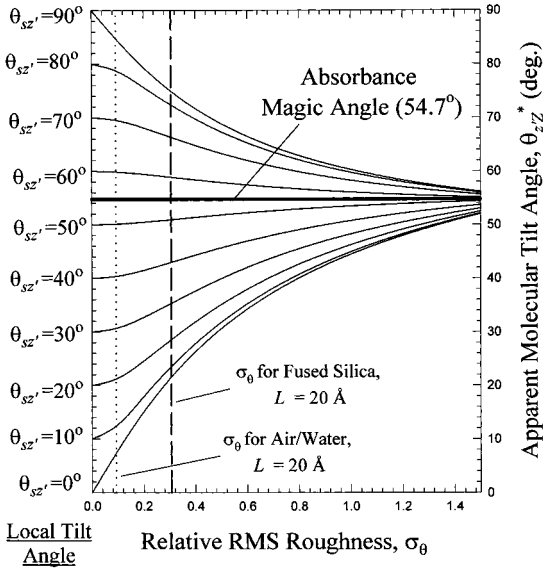

FIGURE 2. Apparent molecular tilt angle, $\theta_{z'Z}$*, plotted as a function of the relative effective surface roughness, σ_θ, for angle-resolved absorbance measurements. Each curve corresponds to a different local molecular orientation angle, $\theta_{sz'}$, given as the *y*-intercept, (i.e., the tilt observed for a perfectly smooth surface). For example, the second curve from the bottom corresponds to a local tilt angle of 10°. Vertical lines indicate the scale-dependent roughness values determined for L = 20 Å for both a mechanically polished fused silica surface[7] (dashed) and the water/air interface[10] (dotted).

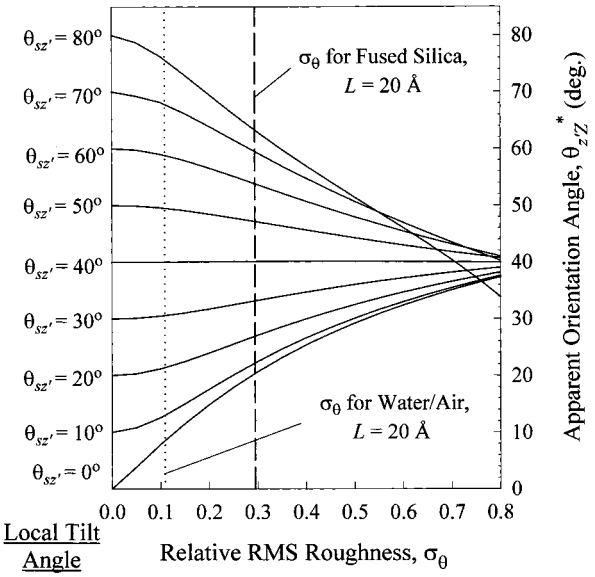

FIGURE 3. Apparent molecular tilt angle, $\theta_{z'Z}$*, plotted as a function of the relative effective surface roughness, σ_θ, for second harmonic generation measurements. Each curve corresponds to a different local molecular orientation angle, $\theta_{sz'}$, given as the *y*-intercept, (i.e., the tilt observed for a perfectly smooth surface). Vertical lines indicate the scale-dependent roughness values determined for L = 20 Å for both a mechanically polished fused silica surface[7] (dashed) and the water/air interface[10] (dotted).

proximated by the following series expansion:[11]

$$K_{sZ} \cong 1 - 2\sigma_\theta^2 + \frac{8}{3}\sigma_\theta^4 - \ldots \qquad (4)$$

Substitution of K_{sZ} (evaluated from the surface/interface roughness using eq 4) into eq 3 in combination with $K_{z'Z}$ (evaluated from macroscopic molecular orientation measurements) allows for determination of the local molecular orientation parameter, $K_{sz'}$.

Shown in Figure 2 is the "apparent" macroscopic molecular orientation angle ($\theta_{z'Z}$*, calculated neglecting roughness effects and assuming a narrow orientation distribution) as a function of the relative effective roughness, σ_θ. Each solid curve corresponds to a different molecular orientation angle with respect to the local surface environment (such that the lowermost curve corresponds to a system in which the molecules orient locally normal to the surface). The convergence to an apparent orientation angle of 55° (i.e., the absorbance magic angle result) in the limit of very rough surfaces is intuitively appealing. As the surface roughness increases, the net distribution in molecular orientation angles is expected to broaden, with the limiting case of a very rough surface yielding the same response as an unoriented system (i.e., the magic angle response). Mathematically, this trend can be explained by inspection of eq 3. As the surface roughness is increased, K_{sZ} approaches a value of $^1/_3$ as all orientation angles for the local surface normal become comparably probable.[12] As a consequence, the macroscopic value for $K_{z'Z}$ approaches a value of $^1/_3$ as well in this case, for which $\theta_{z'Z}^* = \cos^{-1}(1/3)^{1/2} = 54.7°$, regardless of the local molecular orientation (related to $K_{sz'}$).

The two solid vertical lines indicate the values of σ_θ for L = 20 Å, evaluated for a mechanically polished fused silica surface[7] by fractal analysis and for the air/water[10] interface using capillary wave theory. As can be seen from the figure, a monolayer film 20 Å thick oriented with the transition moments all parallel to the local surface normal would produce an apparent macroscopic molecular tilt angle of ~20° for fused silica and ~6° for the air/water interface. In cases where L is less than 20 Å, the influence of surface and interface roughness can be greater still.[11] If roughness effects are neglected, the "macroscopic" orientation measurements may not be representative of local interactions between the molecules and the surface.

Second Harmonic Generation. A similar approach may be used to interpret SHG orientation measurements at surfaces and interfaces. Although the mathematical relations are not as easily expressed in a compact form such as that shown in eq 3, the influence of surface roughness may be evaluated numerically.[13] The results of such calculations are summarized in Figure 3, in which the apparent macroscopic orientation angle is shown as a function of the relative effective roughness, σ_θ. Each curve corresponds to a different local molecular orientation angle calculated in a manner similar to that used in Figure 2 for absorbance measurements. Calculation of the individual curves was independent of any assumptions about the relative magnitudes of the $\beta^{(2)}$ hyperpolarizability tensor elements, requiring only that macroscopic orientation be evaluated from the commonly used ratio of $\langle\cos^3$

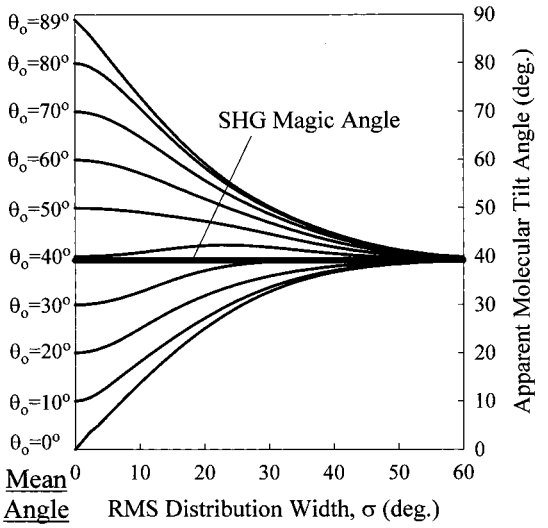

FIGURE 4. Apparent molecular tilt angle (calculated by incorrectly assuming a narrow distribution) for SHG measurements as a function of the width of a Gaussian distribution. The straight line at 39.2° indicates the SHG magic angle.[14]

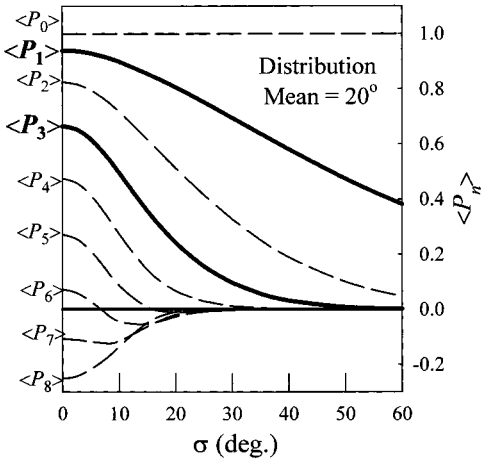

FIGURE 5. First eight Legendre moments of a Gaussian distribution as the distribution is broadened for a mean orientation angle of 20°, chosen arbitrarily. The solid curves indicate the first and third Legendre moments, from which SHG orientation measurements are based (see eq 5).

$\theta_{z'Z}\rangle/\langle\cos\ \theta_{z'Z}\rangle$.[13] Again, the roughness of mechanically polished fused silica can lead to errors as great as ~20° in the interpretation of molecular orientation if the effects of roughness are neglected for $L = 20$ Å (e.g., in the case of a local tilt angle of 0°).

It is interesting to compare the curves shown in Figure 2 for absorbance measurements with those in Figure 3 for SHG measurements. The convergence occurs more quickly with increasing roughness for SHG than for angle-resolved absorbance, as indicated by the factor of ~2 difference in scales in σ_θ. As a result, the influence of roughness is generally greater for SHG orientation measurements than for absorbance measurements. Also of note is the convergence in Figure 3 to an apparent orientation angle of 39° in the limit of a rough surface. The convergence to the magic angle result of 55° in Figure 2 was easily understood, but we found no previous reports of an analogous magic angle result for SHG in the literature. In fact, this apparently anomalous behavior in the limit of rough surfaces led us to propose the existence of a magic angle for SHG.[14]

The SHG Magic Angle

The convergence behavior observed in the limit of rough surfaces (shown in Figure 3) led us to consider more generally the influence of the distribution width on the apparent orientation angle measured by SHG. In Figure 4, the dependence of the apparent orientation angle (defined to be the angle calculated if a narrow distribution is assumed, in this case erroneously) is plotted as a function of the root-mean-square distribution width, σ, for a Gaussian distribution.[14] Each solid line corresponds to a different mean tilt angle. As with the treatment of surface roughness, all calculations are equally valid regardless of the relative magnitudes of the individual $\beta^{(2)}$ molecular hyperpolarizability tensor elements. For narrow distributions, and correspondingly small values of σ, the true mean tilt angle and the apparent tilt angle are in good agreement. However, as the distribution is allowed to broaden, the difference between the true mean tilt angle and the apparent tilt angle generally increases. In all cases, the apparent orientation angle converges to a value of 39.2° in the limit of a broad distribution.

This convergence to 39.2° conflicts with earlier predictions, in which broad orientation distributions were anticipated to produce apparent orientation angles of 35.3°.[15−17] The previous considerations employed partial random distributions in their analyses (i.e., random from 0 to $\pi/2$, and zero from $\pi/2$ to π). However, the partial random distributions failed to accurately predict the known absorbance magic angle of 54.7° as used. On the basis of these discrepancies, we proposed an alternative mathematical explanation by rewriting the SHG orientation parameter, $D_{z'Z}$, in terms of Legendre polynomials:[14]

$$D_{z'Z} = \frac{\langle\cos^3\theta_{z'Z}\rangle}{\langle\cos\ \theta_{z'Z}\rangle} = \frac{2\langle P_3\rangle + 3\langle P_1\rangle}{5\langle P_1\rangle} \qquad (5)$$

where $\langle P_3\rangle$ and $\langle P_1\rangle$ are the mean values of the third and first Legendre polynomials, respectively (i.e., the third and first Legendre moments) and are given by $\langle P_1\rangle = \langle\cos\ \theta_{z'Z}\rangle$ and $\langle P_3\rangle = (5\ \langle\cos^3\ \theta_{z'Z}\rangle - 3\langle\cos\ \theta_{z'Z}\rangle)/2$.[14] In the limit of the third Legendre moment, being much less than the first Legendre moment in eq 5, the orientation parameter, D, is approximately equal to a constant of $^3/_5$. If a narrow distribution is assumed in this case, the apparent orientation angle will be equal to $\arccos(3/4)^{1/2}$, or 39.2°. Consequently, the convergence to an apparent orientation angle of 39.2° in Figure 4 is explained by a more rapid approach to zero of the third Legendre moment compared with the first as the orientation distribution broadens.

The first eight Legendre moments of a Gaussian distribution centered at 20° are shown in Figure 5 as a function of the distribution width, σ. A general trend can be clearly distinguished in the figure, in which the higher Legendre moments systematically approach zero more rapidly that the lower moments as the distribution is

broadened. Similar trends in the Legendre moments were observed for all mean orientation angles investigated, for both Gaussian and Lorentzian distribution functions. The nearly universal more rapid approach to zero of the third Legendre moment compared with the first as the distribution broadens offers an explanation for the convergence to the magic angle result demonstrated in both eq 5 and Figure 4 (and in Figure 3).

This same trend in Legendre moments also explains the faster convergence to the magic angle result with increasing surface roughness for SHG measurements than for absorbance measurements, as demonstrated in Figures 2 and 3. As the surface roughness increases, and correspondingly the distribution in molecular orientation angles broadens, a specific sequence of events is predicted; the SHG response should approach the SHG magic angle result (corresponding to $\langle P_3 \rangle \rightarrow 0$), followed by approach of absorbance measurements to the corresponding magic angle result (corresponding to $\langle P_2 \rangle \rightarrow 0$), and finally loss of all SHG (corresponding to $\langle P_1 \rangle \rightarrow 0$). The first part of this trend is mirrored in Figures 2 and 3, in which convergence to the respective magic angles occurs more rapidly with increasing σ_θ for SHG than for absorbance.

The observation of the SHG magic angle is by no means restricted to only rodlike molecules with dominant $\beta_{z'z'z'}$ hyperpolarizability tensor elements. By inspection of eq 5, the magic angle should be present for any system, provided molecular orientation is expressed in terms of the orientation parameter $D_{z'Z}$ (where $D_{z'Z} \equiv \langle \cos^3 \theta_{z'Z} \rangle / \langle \cos \theta_{z'Z} \rangle$). The orientation of chromophores with a dominant $\beta_{z'x'x'}$ or $\beta_{x'x'z'}$ tensor element, or even multiple contributing tensor elements, is easily and routinely expressed in terms of the orientation parameter given in eq 5.[18] Additionally, the magic angle result will be obtained if the orientation parameter used can be rewritten in the form of eq 5. For example, orientation by SHG is sometimes expressed by $F_{z'Z} = \langle \sin^2(\theta_{z'Z}) \cos(\theta_{z'Z}) \rangle / \langle \cos^3(\theta_{z'Z}) \rangle$, which is equal to $(1/D_{z'Z} - 1)$. In this case, narrow orientation distributions result in $F_{z'Z} \cong \tan^2\langle \theta_{z'Z} \rangle$, while broad distributions lead to a limiting behavior in which $F_{z'Z}$ approaches a constant of $^2/_3$. Erroneous assumption of a narrow orientation distribution for $F_{z'Z}$ results in an apparent orientation angle of $\arctan(2/3^{1/2}) = 39.2°$, again yielding the magic angle result.

The existence of an SHG magic angle highlights the importance of considering both the mean orientation angle and the distribution about that mean in the interpretation of orientation measurements. The observation of an apparent orientation angle of 39° by SHG cannot, in itself, allow for distinction between either a narrow distribution centered at 39° or a broad distribution centered around an arbitrary mean angle.

Combining Angle-Resolved Absorbance and SHG

The importance of both the mean and the width of the orientation distribution in the interpretation of orientation measurements provided the stimulus to combine results from multiple independent orientation measurements. Specifically, orientation measurements by SHG and ARAPD were combined to probe the orientation distributions of both physisorbed and covalently bound surface species.[3]

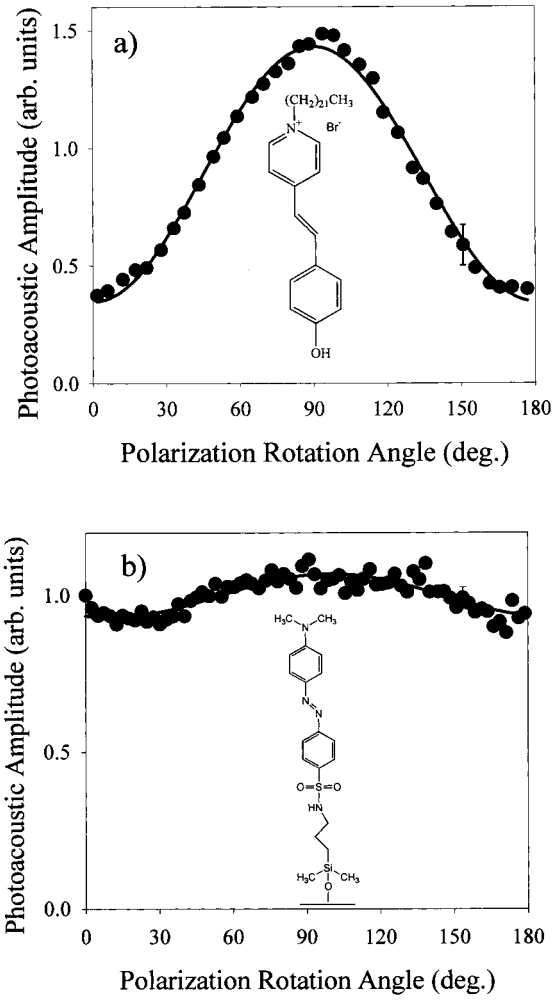

FIGURE 6. Averaged, normalized angle-resolved photoacoustic amplitudes acquired for monolayer films of DPB (a) and submonolayer films of a surface-bound azo dye (b). The chemical structures of the two dyes are inset in each figure. Solid lines are nonlinear fits to the data. A representative error bar ($\pm 1\sigma$) is provided on each curve. The data shown for the azo dye have been corrected for a time-dependent photochemical loss.

ARAPD results for monolayer films of adsorbed 1-docosyl-4-(4-hydroxystyryl)pyridinium bromide (DPB) and a surface-bound azo dye are shown in Figure 6. In each plot, the photoacoustic amplitude (proportional to sample absorbance) is shown as a function of the polarization rotation angle of the 355 nm excitation beam, γ (with $\gamma = 0°$ corresponding to *p*-polarized light). Fits of the data (accounting for reflection, refraction, and the electric fields at the interface) are given by the solid lines.[3]

SHG response curves for DPB and an azo dye were acquired under conditions identical to those used for the ARAPD measurements and are shown in Figure 7 as a function of the polarization rotation angle of a 1064 nm fundamental beam. From fits of the data (given by the solid lines in Figure 7), relative values for the three

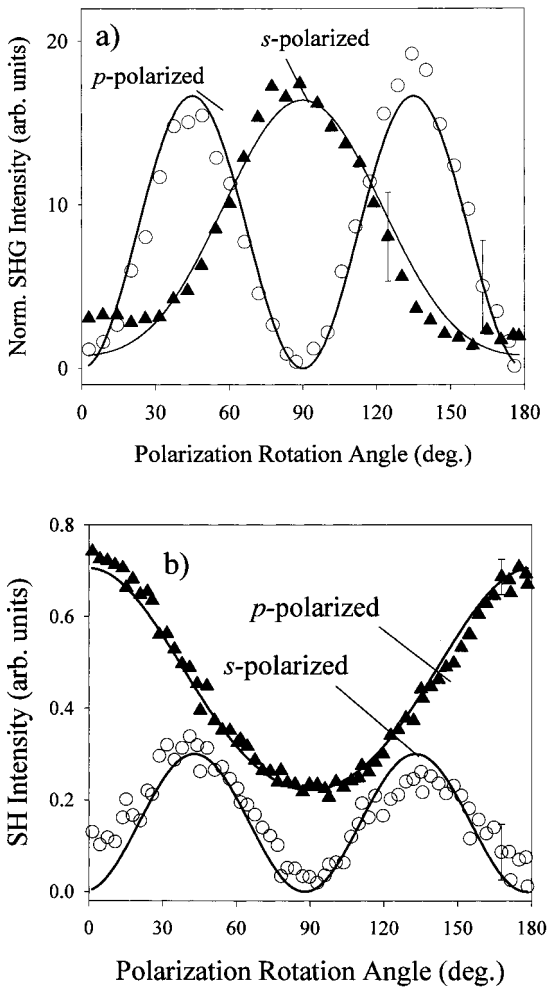

FIGURE 7. Averaged, normalized SHG results acquired for monolayer films of DPB (a) and the azo dye (b). Solid lines are nonlinear fits to the data. A representative error bar ($\pm 1\sigma$) is provided on each curve.

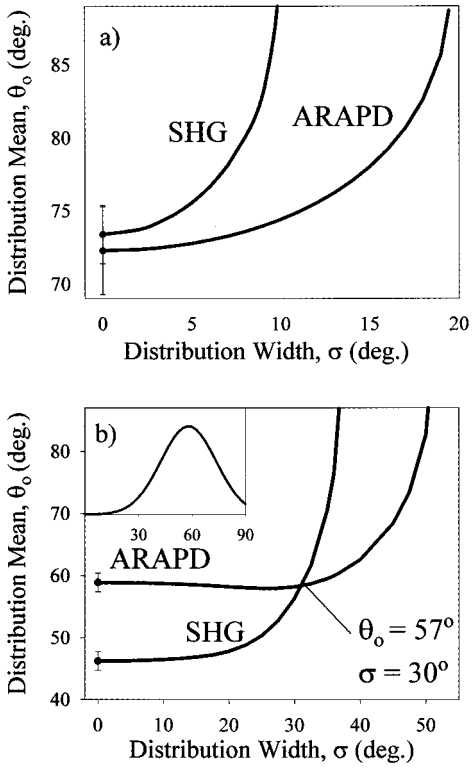

FIGURE 8. Combined SHG and ARAPD molecular orientation measurements to determine both the means (θ_0) and root-mean-square widths (σ) of the orientation distributions for DPB (a) and the azo dye (b). Each curve indicates the range of Gaussian distributions which can yield the corresponding experimental orientation parameter obtained by either SHG or ARAPD orientation measurements alone. The points at which the ARAPD and SHG curves cross represent the distribution means and widths, which are consistent with both sets of measurements. For DPB, the two curves are within error in the limit of a narrow distribution, while for the azo dye the distribution mean is ~57° and the width is ~30°. The corresponding orientation distribution for the azo dye is shown in the inset plot in (b) for angles from 0° to 90°.

independent surface second-order nonlinear tensor elements, χ_{zzz}, χ_{zxx}, and χ_{xxz}, were evaluated.[3]

If the assumption of a narrow molecular orientation distribution is relaxed and a Gaussian distribution is instead assumed, a single measurement is not sufficient to determine both the mean and the width of the angular distribution. This ambiguity can be removed by combining both ARAPD and SHG measurements for a given molecular system. As shown in Figure 8 for a Gaussian distribution, a range of possible solutions satisfies a single measurement, with one extreme being an infinitely narrow distribution and the other a potentially broad distribution. The point at which the ARAPD and SHG curves cross indicates the distribution width and mean, which are consistent with both orientation measurements. These crossover points represent the graphical equivalent of solving two equations with two unknowns. For DPB films, the two spectroscopic measurements yielded nearly identical orientation parameters. From the magnitudes of the experimental errors, it may be concluded that the orientation distribution for the DPB monolayers was centered around 73° with a distribution width of less than ~8° (i.e., the width at which the experimental errors no longer overlap). In contrast, the azo dye yielded a Gaussian distribution mean of 57° with a root-mean-square width of 30°. This distribution is shown in the inset of Figure 8b. Although the assumption of a narrow distribution has been proven accurate for the case of DPB, the same assumption failed to reliably describe the orientation distribution for the azo dye.

The significant difference in distribution widths for DPB and the azo dye system agrees with intuitive arguments for the nature of the orienting interactions in the two cases. For the covalently bound azo dye films, dye molecules are attached specifically to surface hydroxyl groups for a surface coverage of less than 1/10 of a monolayer,[3] suggesting that the predominant orienting interactions are those of the isolated chromophore. A propyl chain near the base of the chromophore allows for a wide range of accessible chromophore orientations for the azo dye, and subsequently a broad orientation distribution. In contrast, the dominating orienting forces for the full monolayer DPB surface films are most likely intermolecular interactions (between adjacent chromophores and/or the long aliphatic hydrocarbon chains).

Assembly of neighboring DPB molecules into highly ordered structures would naturally lead to a high degree of chromophore order as well, and a corresponding narrow orientation distribution.

Orientation-Insensitive SHG Measurements

In addition to determination of molecular orientation, SHG can be employed as a powerful surface-selective probe of surface coverage. In the simplest cases, the second harmonic intensity is directly proportional to the square of the surface number density. Measurement of the SHG response as a function of analyte concentration can then be used to generate adsorption isotherms, while the SHG response measured as a function of time can yield kinetic information. Furthermore, the surface selectivity of second-order nonlinear processes generally allows for negligible contributions from the bulk, in contrast to linear techniques such as absorbance and fluorescence. However, an often overlooked complication in such measurements can arise if the orientation distribution changes as a function of surface coverage. For example, a surface system might undergo a two-dimensional phase transition as the surface number density increases, with an accompanying change in orientation. In such cases, the change in SHG intensity with time or concentration is a convolution of changes in both surface number density and molecular orientation.

In absorbance measurements, such complications are easily remedied by configuring the instrument such that the surface electric field vector of the excitation beam is oriented at an angle of 54.7° with respect to the surface normal (i.e., the magic angle).[11,12] Under these conditions, absorbance measurements are independent of molecular orientation. Demonstration of the SHG magic angle raised the intriguing possibility of a similar effect in nonlinear optical measurements, in which judicious choice of the experimental configuration could yield SHG measurements insensitive to changes in orientation. To investigate this possibility, theoretical response curves for the predicted *p*-polarized SHG response as a function of the fundamental polarization rotation angle were generated for dominant $\beta_{z'z'z'}$, $\beta_{z'x'x'}$, and $\beta_{x'x'z'}$ molecular hyperpolarizabilities.[19] Furthermore, this methodology (presented in greater detail in refs 19 and 20) may be easily extended to systems in which multiple tensor elements are significant. An example of such a plot is shown in Figure 9 for a dominant $\beta_{z'z'z'}$ molecular hyperpolarizability tensor element (typical for rodlike chromophores). Each solid line in Figure 8 corresponds to a different apparent molecular orientation angle.

Two aspects of Figure 9 are worth special attention. Most significantly for this discussion, several of the curves for molecular tilt angles less than ~50° cross at a polarization rotation angle of the fundamental beam of ~63°. As a result, measurement of the *p*-polarized SHG intensity acquired for a fundamental polarization rotation angle of 63° in a total internal reflection geometry will yield comparable *p*-polarized SHG intensities for essentially any

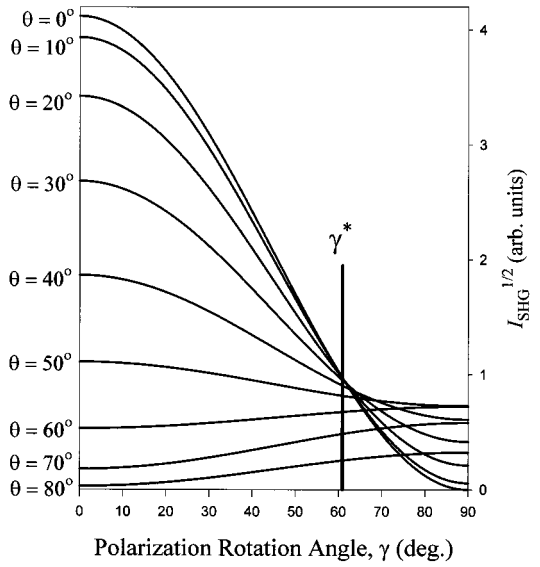

FIGURE 9. Theoretical *p*-polarized SHG response curves calculated for several apparent orientation angles for a dominant $\beta_{z'z'z'}$ molecular hyperpolarizability tensor element. Curves were calculated using the fitting coefficients for a total internal reflection cell.[3] Each curve was calculated assuming to a different apparent orientation angle, indicated on the left margin. The solid vertical line is the appropriate value of γ^* calculated using eq 6.

orientation angle between 0° and 50°. Under these experimental conditions, the detected SHG intensity becomes largely independent of molecular orientation, such that measured changes in intensity can be attributed solely to changes in surface coverage. The other important aspect of the curves in Figure 9 is that measurement of the *p*-polarized SHG intensity for a *p*-polarized fundamental (i.e., $\gamma = 0°$), as is routinely done experimentally, effectively maximizes the sensitivity of the detected intensity to changes in orientation, and correspondingly the potential for errors from changes in orientation.

Provided that the mean tilt angle of the surface chromophores is reasonably small (such that $\langle \sin^2(\theta_{z'Z}) \cos(\theta_{z'Z})\rangle \cong \langle \theta_{z'Z}^2\rangle$ and $\langle \cos^3(\theta_{z'Z})\rangle \cong 1 - {}^3/_2\langle \theta_{z'Z}^2\rangle$),[19] approximate values for the orientation insensitive polarization rotation angle of the fundamental beam (hereby designated γ^*) can be generated. For a dominant $\beta_{z'z'z'}$ molecular hyperpolarizability tensor element, γ^* is given by[19]

$$\gamma^* = \cos^{-1}\left(\frac{s_5}{3s_4 + s_5 - s_2 - s_3}\right)^{1/2} \qquad (6)$$

in which each of the s_n terms is a product of geometric terms and Fresnel factors ($s_2 = L_{XX}^{2\omega} L_{XX}^{\omega} L_{ZZ}^{\omega} \sin(2\theta^{\omega}) \cos\theta^{2\omega}$, $s_3 = L_{ZZ}^{2\omega}(L_{XX}^{\omega})^2 \cos^2\theta^{\omega} \sin\theta^{2\omega}$, $s_4 = L_{ZZ}^{2\omega}(L_{ZZ}^{\omega})^2 \sin^2\theta^{\omega} \sin\theta^{2\omega}$, and $s_5 = L_{ZZ}^{2\omega}(L_{YY}^{\omega})^2 \sin\theta^{2\omega}$, where θ^{ω} is the angle of incidence of the fundamental beam at the interface, $\theta^{2\omega}$ is the angle of reflection of the second harmonic, and L^{ω} and $L^{2\omega}$ are linear and nonlinear Fresnel factors, respectively).[3] The Fresnel factors relate the electric field components at the interface (indicated by the subscripts) to the incident and detected fields (explicit expressions for the Fresnel factors used in these investigations and a description of the model used to determine them can be

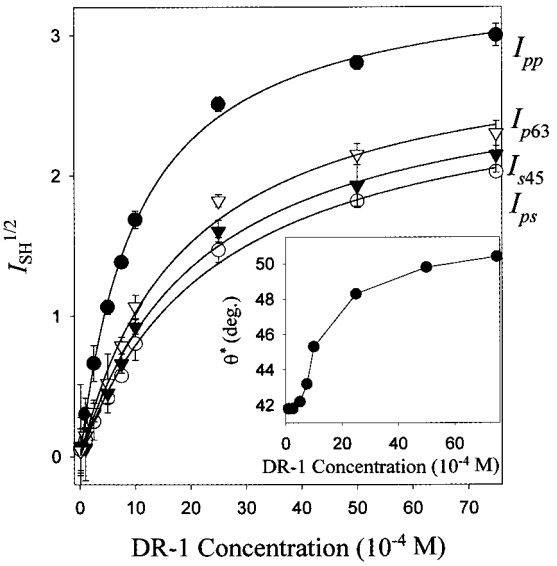

FIGURE 10. Adsorption isotherms for DR-1 on glass (from methylene chloride solutions) measured under different polarization conditions: I_{pp}, ●; I_{p63}, ▽; I_{s45}, ▼; and I_{ps}, ○. The solid lines are Langmuir fits to the data, yielding the following adsorption equilibrium constants: $K_{pp} = 940 \pm 40$ M^{-1}, $K_{p63} = 540 \pm 60$ M^{-1}, $K_{s45} = 470 \pm 50$ M^{-1}, and $K_{ps} = 410 \pm 40$ M^{-1}, where the subscripts indicate the polarization combination under which the data were acquired. The apparent orientation angle, θ^*, as a function of concentration is shown in the inset, evaluated from the combined intensity measurements.

found in ref 3). Expressions analogous to eq 6 have also been generated for dominant $\beta_{z'x'x'}$ and $\beta_{x'x'z'}$ molecular hyperpolarizability tensor elements.[19] By use of expressions such as those given in eq 6, the orientation-insensitive polarization rotation angle of the fundamental beam, γ^*, can be easily estimated for essentially any experimental configuration.

The orientation-insensitive polarization rotation angle, γ^*, given for rodlike molecules by eq 6, should not be confused with the SHG magic angle of 39.2° described in a previous section. The SHG magic angle is a constant describing the apparent orientation angle obtained by SHG if a broad orientation distribution is erroneously assumed to be narrow and is valid regardless of the molecular hyperpolarizability tensor $\beta^{(2)}$. In contrast, γ^* changes depending on the dominant molecular hyperpolarizability tensor element[19] and with the experimental configuration (e.g., with the angle of incidence and refractive indices of the substrate and ambient media). The two angles describe distinctly separate and unique phenomena.

Adsorption isotherm and kinetics investigations can, in many cases, be made without significant complications from coverage-dependent changes in orientation simply by "parking" the fundamental polarization rotation angle at γ^* prior to acquisition of second harmonic intensity measurements. Such measurements are shown in Figure 10 for adsorption isotherms of disperse red 1 (DR-1) on glass from methylene chloride solutions.[20] Isotherm measurements were acquired under four different polarization conditions, I_{pp}, I_{ps}, I_{s45}, and the orientation-insensitive

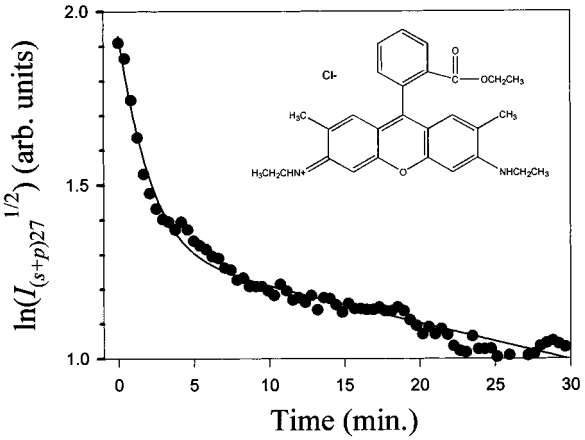

FIGURE 11. Desorption kinetics for rhodamine-6G (10^{-3} M in methylene chloride) from glass. The chemical structure of rhodamine-6G is inset in the figure. The solid line is a biexponential fit to the data. From the fit, the two decay constants were $k_1 = 0.59 \pm 0.03$ min^{-1} and $k_2 = 0.0105 \pm 0.0006$ min^{-1}.

polarization condition (in this case, I_{p63}), in which the first subscript indicates the polarization state of the second harmonic and the second subscript the polarization state of the fundamental (either *s*-polarized, *p*-polarized, or an intermediate polarization rotation angle given in degrees). Solid lines are fits to the data according to the Langmuir adsorption model.[21] Each fit yields a different value for the equilibrium constant for adsorption, provided in the figure caption. The differences between the equilibrium constants evaluated under different polarization conditions can be attributed to a coverage-dependent orientation for DPB, as indicated by the change in apparent orientation angle with coverage shown in the inset plot.

If the adsorption data are corrected for the apparent molecular orientation angle at each point in the curve, and the combined results are fit to a Langmuir adsorption isotherm, an equilibrium constant for adsorption of 500 $\pm$ 40 M^{-1} is obtained. This orientation-angle-corrected value is within error of the value obtained under the orientation-insensitive conditions (i.e., 540 $\pm$ 60 M^{-1} for I_{p63} in Figure 10) and differs by almost 100% with the value obtained for a *p*-polarized second harmonic and a *p*-polarized fundamental (i.e., 940 $\pm$ 40 M^{-1}). These results are in excellent agreement with theoretical predictions based on the results shown in Figure 9, in which errors associated with coverage-dependent changes in orientation are generally minimized using the polarization-insensitive experimental configuration and maximized for measurements of I_{pp} alone for a $\beta_{z'z'z'}$ dominated system.

The utility of an orientation-insensitive methodology for SHG coverage measurements is best illustrated in kinetics studies. Shown in Figure 11 are kinetics measurements for rhodamine 6G desorption from glass in contact with methylene chloride; these data were acquired under the appropriate polarization-insensitive configuration (in this case, evaluated for a dominant $\beta_{x'x'z'}$ tensor element).[19,20] The solid line is a best fit of the data to a biexponential decay. Acquisition of comparably accurate results by more traditional means would require at least three independent measurements under different polar-

ization conditions at each data point in the desorption curve and subsequent correction of the data for molecular orientation.

Summary

Recent studies in our laboratory have been directed toward a better understanding of molecular orientation and orientation measurements at surfaces and interfaces. Several recent inquiries were briefly described, including a method to quantify and correct for roughness effects in linear and nonlinear orientation measurements, the discovery of an SHG magic angle, a new approach to evaluate the means and widths of orientation distributions by combining absorbance and SHG measurements, and a methodology allowing for SHG measurements insensitive to changes in molecular orientation.

The authors gratefully acknowledge funding from the National Science Foundation.

References

(1) Doughty, S. K.; Rowlen, K. L. Molecular-Orientation at Dielectric Surfaces by Angle-Resolved Photoacoustic-Spectroscopy. *J. Phys. Chem.* **1995**, *99*, 2143−2150.
(2) Doughty, S. K.; Simpson, G. J.; Rowlen, K. L. Evolution of Orientation in the Growth of Azo Dye Zirconium Phosphate-Phosphonate Multilayers. *J. Am. Chem. Soc.* **1998**, *120*, 7997−7998.
(3) Simpson, G. J.; Westurbuhr, S. G.; Rowlen, K. L. Molecular Orientation and Angular Distribution Probed by Angle-Resolved Absorbance and Second Harmonic Generation. *Anal. Chem.* **2000**, *72*, 887−898.
(4) Shen, Y. R. Optical Second Harmonic Generation at Interfaces. *Annu. Rev. Phys. Chem.* **1989**, *40*, 327−350.
(5) Corn, R. M.; Higgins, D. A. Optical Second Harmonic Generation as a Probe of Surface Chemistry. *Chem. Rev.* **1994**, *94*, 107−125.
(6) McGilp, J. F. Insitu Optical Spectroscopy of Surfaces and Interfaces with Submonolayer Resolution. *Appl. Surf. Sci.* **1993**, *63*, 99−105.
(7) Simpson, G. J.; Rowlen, K. L. Quantification of "Local" Surface Orientation: Theory and Experiment. *J. Phys. Chem. B* **1999**, *103*, 1525−1531.
(8) Simpson, G. J.; Sedin, D. L.; Rowlen, K. L. Surface Roughness by Contact versus Tapping Mode Atomic Force Microscopy. *Langmuir* **1999**, *15*, 1429−1434.
(9) Palasantzas, G. Roughness Spectrum and Surface Width of Self-Affine Fractal Surfaces Via the K-Correlation Model. *Phys. Rev. B* **1993**, *48*, 14472−14478.
(10) Simpson, G. J.; Rowlen, K. L. Evaluation of Molecular-Scale Roughness at Liquid Interfaces. *Chem. Phys. Lett.* **1999**, *309*, 117−122.
(11) Simpson, G. J.; Rowlen, K. L. Molecular Orientation at Surfaces: Surface Roughness Contributions to Measurements Based on Linear Dichroism. *J. Phys. Chem. B* **1999**, *103*, 3800−3811.
(12) Michl, J.; Thulstrup, E. K. *Spectroscopy with Polarized Light*; VCH Publishers: Weinheim, 1995; Chapter 5.
(13) Simpson, G. J.; Rowlen, K. L. Influence of Substrate Roughness on Orientation Measurements by Second Harmonic Generation. *Chem. Phys. Lett.* **2000**, *317*, 276−281.
(14) Simpson, G. J.; Rowlen, K. L. An SHG Magic Angle: Dependence of Second Harmonic Generation Orientation Measurements on the Width of the Orientation Distribution. *J. Am. Chem. Soc.* **1999**, *120*, 7997−7998 and references therein.
(15) Tamburello-Luca, A. A.; Hebert, P.; Brevet, P. F.; Girault, H. H. Resonant-Surface Second-Harmonic Generation Studies of Phenol Derivatives at Air/Water and Hexane/Water Interfaces. *J. Chem. Soc., Faraday Trans.* **1996**, *92*, 3079−3085.
(16) Higgins, D. A.; Abrams, M. B.; Byerly, S. K.; Corn, R. M. Resonant Second Harmonic-Generation Studies of *p*-Nitrophenol Adsorption at Condensed-Phase Interfaces. *Langmuir* **1992**, *8*, 1994−2000.
(17) Corn, R. M.; Higgins, D. A. Molecular Orientation in Thin Films as Probed by Optical Second Harmonic Generation. In *Characterization of Organic Thin Films*; Ulman, A., Ed.; Butterworth-Heinemann: Stoneham, MA, 1995; Chapter 12.
(18) Dick, B. Irreducible Tensor Analysis of Sum-Frequency and Difference-Frequency-Generation in Partially Oriented Samples. *Chem. Phys.* **1985**, *96*, 199−215.
(19) Simpson, G. J.; Rowlen, K. L. Orientation Insensitive Methodology for Second Harmonic Generation. Part I: Theory. *Anal. Chem.* **2000**, *72*, 3399−3406.
(20) Simpson, G. J.; Rowlen, K. L. Orientation Insensitive Methodology for Second Harmonic Generation. Part II: Application to Adsorption Isotherm and Kinetics Measurements. *Anal. Chem.* **2000**, *72*, 3407−3411.
(21) Steinfeld, J. I.; Francisco, J. S.; Hase, W. L. *Chemical Kinetics and Dynamics*; Prentice Hall: Englewood Cliffs, NJ, 1989; Chapter 5.

AR0000307